AGU PUBLICATIONS

JGR

Journal of Geophysical Research: Atmospheres

RESEARCH ARTICLE

10.1002/2017JD027870

Key Points:
- Tropopause folds during northern summer occur as a result of monsoon dynamics
- Tropopause folds are associated with decreased likelihood of extreme rainfall upstream while increased likelihood downstream
- Tropopause folds vary with monsoon intensity

Supporting Information:
- Supporting Information S1

Correspondence to:
Y. Wu,
yutianwu@ldeo.columbia.edu

Citation:
Wu, Y., Chen, G., Taylor, L., & Zhang, P. (2018). On the linkage between the Asian summer monsoon and tropopause folds. *Journal of Geophysical Research: Atmospheres*, *123*, 2037–2049. https://doi.org/10.1002/2017JD027870

Received 10 OCT 2017
Accepted 31 JAN 2018
Accepted article online 6 FEB 2018
Published online 22 FEB 2018

On the Linkage Between the Asian Summer Monsoon and Tropopause Folds

Yutian Wu[1], Gang Chen[2], Lindsey Taylor[3], and Pengfei Zhang[3]

[1]Lamont-Doherty Earth Observatory, Columbia University, Palisades, NY, USA, [2]Department of Atmospheric and Oceanic Sciences, University of California, Los Angeles, CA, USA, [3]Department of Earth, Atmospheric, and Planetary Sciences, Purdue University, West Lafayette, IN, USA

Abstract This study uses a set of idealized aquaplanet model experiments to investigate the linkage between the Asian summer monsoon circulation and tropopause fold activity. It is found that folds tend to occur on the northwestern side of the upper-level anticyclone associated with the monsoon circulation and are generated due to intensified monsoon circulation and resulting intensified subsidence. In addition, the impact of tropopause folds on extreme rainfall events is also examined. It is found that while the likelihood of extreme rainfall is largely decreased at and upstream of the occurrence of folds, the likelihood is significantly increased downstream. This pattern of suppression of extreme rainfall upstream and promotion downstream also persists for about 1–2 days, which likely suggests a positive feedback between extreme rainfall downstream and tropopause folds. Finally, changes in tropopause folds with monsoon intensity are also discussed.

1. Introduction

Tropopause folds are important dynamical processes of troposphere-stratosphere coupling and are characterized by deformation of the tropopause and intrusion of stratospheric air into the troposphere (e.g., Danielsen, 1968; Keyser & Shapiro, 1986; Reed, 1955; Reed & Danielsen, 1959; Shapiro, 1980, 1981). It is well known that tropopause folds are primarily driven by upper-level frontogenesis and ageostrophic vertical motion (e.g., Keyser & Shapiro, 1986, and references therein; Bourqui & Trepanier, 2010; Skerlak et al., 2015; Thorpe, 1997). As a result, tropopause folds play an important role in stratosphere-troposphere exchange of ozone and other chemical constituents (Holton et al., 1995; Lamarque & Hess, 1994; Sprenger et al., 2003; Stohl et al., 2003, and references therein). Furthermore, because folds are associated with development of upper-level positive potential vorticity (PV) anomalies, they could possibly contribute to rapid cyclogenesis, deep convective storms, and other severe weather events (e.g., Browning & Reynolds, 1994; Browning & Golding, 1995; Goering et al., 2001; Griffiths et al., 2000; Thorpe, 1997; Uccellini, 1990; Wernli et al., 2002).

Previous studies on tropopause folds mostly focused on the extratropical folds (e.g., Rao & Kirkwood, 2005; Sprenger et al., 2003) and much less on the summer folds in the subtropics. However, recent studies by Tyrlis et al. (2014) and Skerlak et al. (2015) examined the climatology of tropopause folds using the ERA-Interim reanalysis and found a “hot spot” of summertime fold activity over the eastern Mediterranean and the Middle East. The contribution from these folds in carrying ozone-rich stratospheric air to the observed tropospheric summer ozone pool over the eastern Mediterranean is also discussed in many other studies (e.g., Kourtidis et al., 2002; Lelieveld et al., 2002; Roelofs & Lelieveld, 1997; Roelofs et al., 2003). Recent study of Yang et al. (2016) calculated the isentropic stratosphere-troposphere exchange and found a noticeable peak in stratosphere-to-troposphere exchange of ozone in late spring and early summer in the Northern Hemisphere (NH), likely associated with monsoon circulation.

Tyrlis et al. (2014) further argued from empirical evidence that recent upward trend of the fold activity over the eastern Mediterranean and the Middle East is controlled by the advanced onset of the South Asian summer monsoon in recent years and suggested a possible linkage between the Asian summer monsoon and tropopause fold activity. However, the dynamical mechanism is not fully understood. Some previous studies suggested Rossby wave breaking (RWB) as a possible mechanism for tropopause folds, and in particular, RWB may take a form of tropopause folds in the vertical direction (e.g., Allen et al., 2009; Postel & Hitchman, 1999; Skerlak et al., 2015). However, during NH summer, tropopause folds and RWB do not take place at the

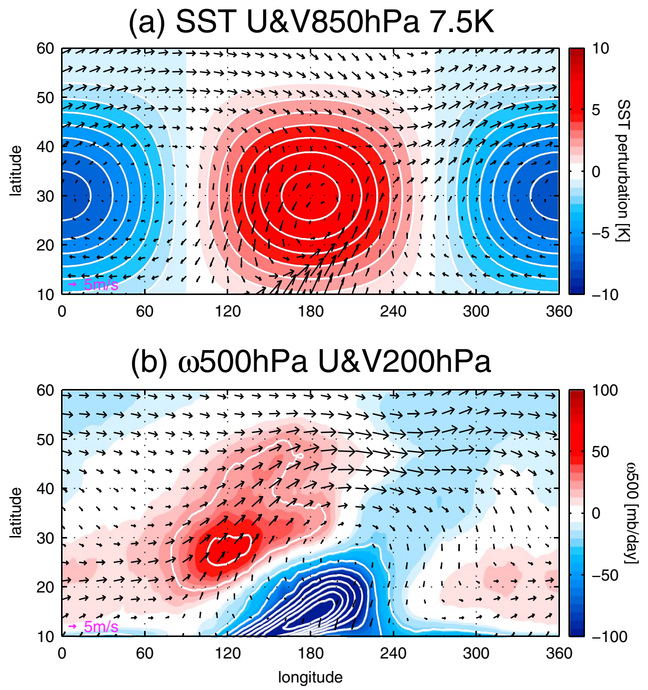

Figure 1. In idealized aquaplanet 7.5 K model experiment, (a) zonal wave-1 sea surface temperature (SST) perturbation that is maximized at 30°N with a maximum intensity of 7.5 K (in unit of kelvin, plotted in color shadings and contours with contour interval of 1 K) and 850 hPa horizontal velocity (vectors) and (b) 500 hPa vertical velocity (in unit of mb/d, plotted in color shadings and contours with CI = 25 mb/d) and 200 hPa horizontal velocity (vectors).

same geographical location. More specifically, while tropopause folds occur over the eastern Mediterranean and the Middle East (e.g., Skerlak et al., 2015), RWB events maximize over the North Pacific and North Atlantic Oceans (e.g., Homeyer & Bowman, 2013; Kunz et al., 2015; Postel & Hitchman, 1999).

Therefore, the main questions we aim to address in this study are as follows: 1. What is the linkage between the Asian summer monsoon and tropopause folds? 2. Can we simulate and understand tropopause folds using idealized numerical model experiments? 3. What is the linkage between tropopause folds and extreme weather events? 4. How do tropopause folds vary with Asian summer monsoon intensity? This paper is organized as follows. In section 2, we describe the reanalysis data set, idealized model experiments, and identification methods for tropopause folds and RWB. In section 3, we present the results in idealized model experiments and discuss the dynamical mechanism and impact of tropopause folds. Section 4 concludes the paper.

2. Data and Methods

2.1. ERA-Interim Reanalysis

For observations, we use 6-hourly data during 1979–2015 from the ERA-Interim reanalysis produced by the European Centre for Medium-Range Weather Forecasts (Dee et al., 2011). In particular, we use zonal wind, meridional wind, and temperature on a 0.75° longitude by 0.75° latitude grid and hybrid model levels to calculate potential temperature and PV, which are further used for the identification of tropopause folds (to be discussed later). Six-hourly PV at 200 hPa is also used for the identification of RWB (to be discussed later).

2.2. Idealized Model Experiments

In addition to observations, we also perform a set of idealized numerical model experiments using the National Center for Atmospheric Research Community Atmosphere Model version 5 aquaplanet configuration with prescribed sea surface temperatures (SSTs) (Neale et al., 2012). The model is integrated at about 0.9° longitude by 0.9° latitude with 30 model levels in the vertical, and the experiment setup is similar to Shaw (2014) and Wu and Shaw (2016). The control experiment (namely "CTRL" run) prescribes a zonally symmetric SST with maximum SST located at 10°N (see Figure S1a in the supporting information). The perturbation experiment (namely "7.5 K" run) is designed to mimic the NH subtropical land-ocean heating contrast associated with the summer monsoon and further adds a subtropical zonal wave-1 SST perturbation that is centered at 30°N and has an amplitude of 7.5 K (see Figure S1b in the supporting information). Similar responses were found when a subtropical zonal wave-2 SST perturbation was introduced (Shaw, 2014; Wu & Shaw, 2016), and this study focuses on the zonal wave-1 perturbation experiment for the sake of simplicity. In addition, in order to examine the sensitivity of the results to the amplitude of the SST perturbation, two additional perturbation experiments are also performed with a SST perturbation amplitude of 5 K and 10 K, respectively (namely "5 K" run and "10 K" run). The CTRL, 5 K, and 10 K simulations are integrated for 10 years. Since most of the results to be presented focus on the 7.5 K run, this simulation is integrated for 20 years for the robustness of the results. All the analysis is based on the entire length of the simulations with the first 2 years of "spin-up" skipped, and we save 6-hourly zonal wind, meridional wind, temperature, specific humidity, precipitation, and surface pressure.

Consistent with previous studies (e.g., Shaw, 2014; Wu & Shaw, 2016), as shown in Figure 1, the 7.5 K experiment is able to simulate a monsoon-like circulation with a low-level cyclonic circulation coupled to a strong ascent right above. A descent is seen on the northwestern side of the ascent, as a result of westward Rossby wave propagation, and is further coupled to an upper-level anticyclone (Gill, 1980; Rodwell & Hoskins, 1996; 2001).

2.3. Identification of Tropopause Folds

For the identification of tropopause folds, we make use of the algorithm code that is developed by Skerlak et al. (2015). The algorithm code first identifies and labels the atmospheric air as five types including 1 = troposphere, 2 = stratosphere, 3 = stratospheric cutoff or diabatically produced PV anomaly, 4 = tropospheric

10.1002/2017JD027870

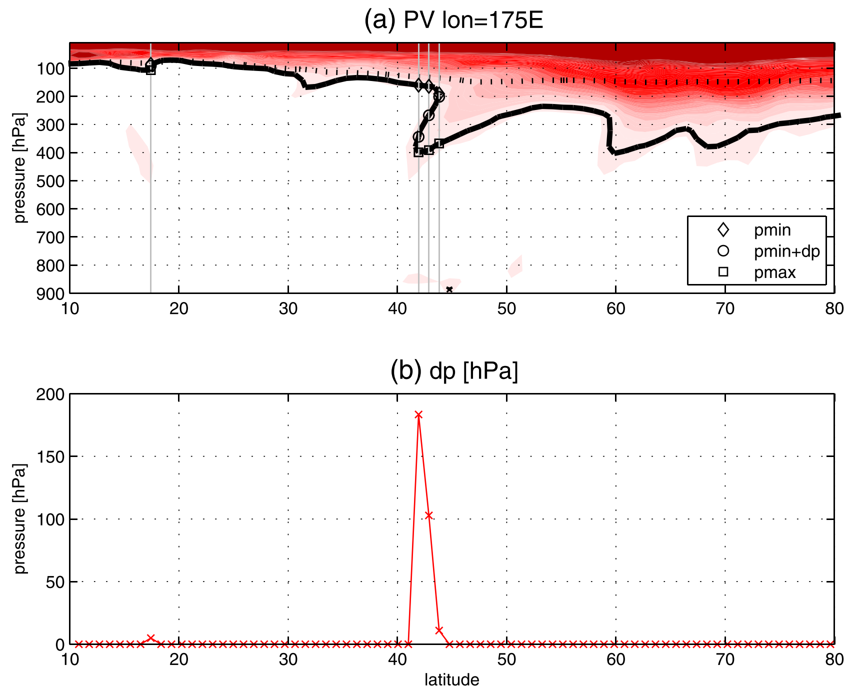

Figure 2. An example of tropopause fold in idealized aquaplanet 7.5 K model experiment (model setup shown in Figure 1) with (a) potential vorticity (PV) values (shown in color shadings) and (b) vertical extent of tropopause fold (dp) at 175E. Also shown in (a) are 2 PVU surface (black thick line), 380 K surface (black dotted line), and tropopause folds with multiple vertical crossings denoted by $p_{\min}$ (diamonds), $p_{\min}$ + dp (circles), and $p_{\max}$ (squares).

cutoff, and 5 = surface-bound PV anomaly based on the PV values and the 2 PVU dynamical tropopause (or 380 K tropopause, whichever is the lowest in altitude). Then tropopause folds are defined as multiple crossings of the dynamical tropopause in a vertical profile if, from highest to lowest altitude, there are subsequent transitions from labels 2 to 1, then from 1 to 2, and finally from 2 to 1 (a schematic can be seen in Figure 1 of Skerlak et al., 2015).

Figure 2 shows an example of the identification of tropopause folds in the 7.5 K experiment. The algorithm outputs the pressure levels of multiple vertical crossings and the vertical extent of the tropopause folds.

2.4. Identification of RWB

For the identification of RWB, we use an algorithm that is used in Rivière (2009) and Lu et al. (2014). This RWB algorithm is applied to 6-hourly PV at 200 hPa, and globe-circling contours are first identified. Then the algorithm searches for overturning contours, and anticyclonic wave breaking (AWB) is identified when the contours overturn anticyclonically while cyclonic wave breaking (CWB) is found when the contours overturn cyclonically, similar to other algorithms used in previous studies (e.g., Homeyer & Bowman, 2013; Strong & Magnusdottir, 2008).

3. Results

3.1. Simulated Folds in Idealized Experiments

First of all, Figure 3a shows the observed frequency of tropopause folds during northern summer using the ERA-Interim reanalysis data averaged over 1979–2015. This is similar to Figure 5 of Skerlak et al. (2015), and during northern summer, maximum frequency of tropopause folds occurs over the Mediterranean, Middle East, and north Tibetan Plateau (about 10–20% or equivalently 9–18 days on average during boreal summer) and to a lesser extent western North America (about 2.5% or about 2–3 days on average). Figure 3a also shows the upper-level horizontal circulation, and as can be seen, tropopause folds tend to take place on the northwestern side of the upper-level anticyclone.

In the CTRL run with zonally symmetric SSTs, there is no occurrence of tropopause folds (not shown). Figure 3b shows the results in the idealized aquaplanet 7.5 K experiment as a result of zonally asymmetric heating that mimics the contrast between warm land and cold ocean in summer. The figure is shifted by 120° longitude

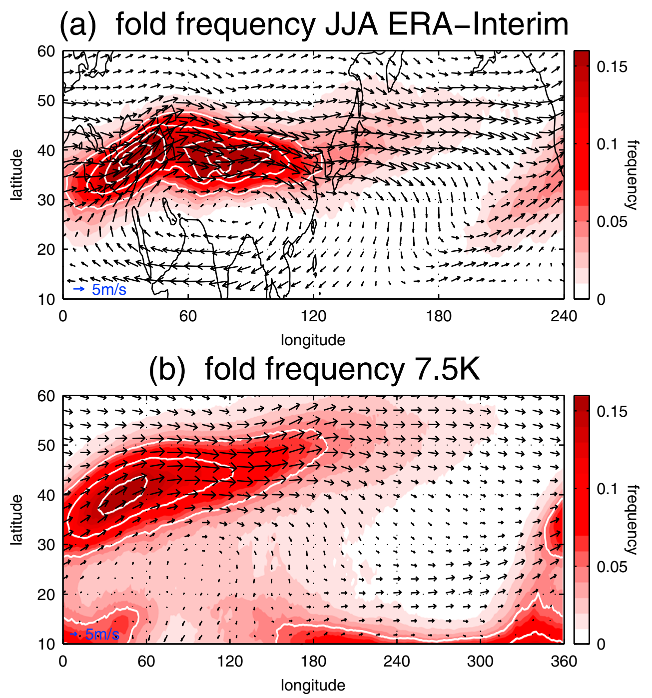

Figure 3. Tropopause fold frequency in (a) ERA-Interim reanalysis during June-July-August (JJA) and (b) idealized 7.5 K model experiment (shown in color shadings and contours with CI = 0.05). Also shown are 200 hPa horizontal wind fields (vectors). The result from reanalysis is shown over 0°–240°E so that the size of the forcing domain and the fold response is better comparable to that of the idealized run. (b) Shifted by 120° longitude to the west as compared to Figure 1 in order to better align with Figure 3a.

to the west as compared to Figure 1 in order to better compare with the observational results in Figure 3a. To leading order, the simulated folds are similar to those in observations in both location and magnitude: simulated folds also tend to happen on the northwestern flank of the upper-level anticyclone with maximum frequency about 10–15%. But differences can be seen between the observed and simulated folds. For example, the simulation underestimates the tropopause fold frequency as compared to observations, and additionally, the idealized aquaplanet experiment produces a single maximum in tropopause fold frequency while the observations show two splitted maxima. The two splitted maxima of tropopause fold occurrence in reanalysis could likely be due to the two modes of variability of the South Asia High, that is, the Tibetan Mode and the Iranian Mode (e.g., Zhang et al., 2002) which are absent in idealized aquaplanet model experiments. In fact, the locations of maximum fold occurrence correspond well with the two modes shown in Figure 3 of Zhang et al. (2002). In summary, the idealized aquaplanet model experiments are able to capture the key features of the tropopause folds as in observations and both observations and idealized experiments show that there is a preferred location for the occurrence of the tropopause folds during northern summer.

3.2. Dynamical Mechanisms and Relationship With RWB

Next with the idealized aquaplanet simulations, we examine the dynamical mechanism underlying the occurrence of tropopause folds during northern summer. First, we make a composite of tropopause folding events and examine the surrounding circulation anomaly by removing climatological mean circulation in the 7.5 K run in the neighborhood of 40° longitude and 20° latitude. As shown in Figures 4a and 4b, tropopause folding activity is typically associated with an anomalously intensified descent, which is consistent with previous studies on tropopause folds (e.g., Keyser & Shapiro, 1986 and references therein; Bourqui & Trepanier, 2010; Skerlak et al., 2015; Thorpe, 1997). This descent anomaly is strongly coupled to a southward flow anomaly right below and an intensified low-level cyclonic circulation and ascent downstream (Figure 4b) as well as a northward flow anomaly right above and an intensified upper-level anticyclonic circulation (Figure 4a). A dipole of PV anomaly is also seen in the upper troposphere and lower stratosphere with a positive PV anomaly in the north that is likely of stratospheric origin (Figure 4a). Similar results are also found in the ERA-Interim reanalysis (not shown). Therefore, these results suggest that tropopause folds occur as a result of intensified monsoon circulation and resulting subsidence on the northwestern side.

As discussed in section 1, some studies have linked the occurrence of tropopause folds in the vertical direction to RWB in the horizontal direction (e.g., Allen et al., 2009; Postel & Hitchman, 1999; Skerlak et al., 2015). However, here we show that tropopause folds and RWB take place in different geographical locations during northern summer and both might likely occur as a result of monsoon dynamics. First, in reanalysis data sets, maximum AWB is found to occur over the eastern North Pacific Ocean and eastern Europe and does not overlap with maximum occurrence of tropopause folds (see Figure S2 in the supporting information, and the results are consistent with Figure 9a of Homeyer & Bowman, 2013, for example). Figure 5a shows the frequency of AWB and tropopause folds in the idealized aquaplanet experiment. Similar results are also found in idealized experiment in which AWB does not nearly overlap with tropopause folds but instead occurs downstream (i.e., 180–360°E, 30–50°N) and to a lesser extent upstream of the upper-level anticyclone (i.e., 0–60°E, 40–50°N). CWB is not discussed here: CWB takes place at higher latitudes during northern summer in observations and occurs much less frequent than AWB in idealized experiments (not shown). It is also noted that the maximum frequency of folds is about 15%, but the maximum frequency of AWB is about 5%. In addition, to illustrate how AWB varies with monsoon circulation, Figure 5b shows the regression of AWB and tropopause folds on the monsoonal rising motion. It can be seen that as monsoon circulation becomes intensified with stronger ascent, tropopause folds become more likely, due to the compensating stronger descent, and also shift slightly to the west. For the AWB upstream of the upper-level anticyclone, the frequency decreases strongly and shifts slightly to the west. And for the AWB downstream, there is generally a westward shift and waves tend to break

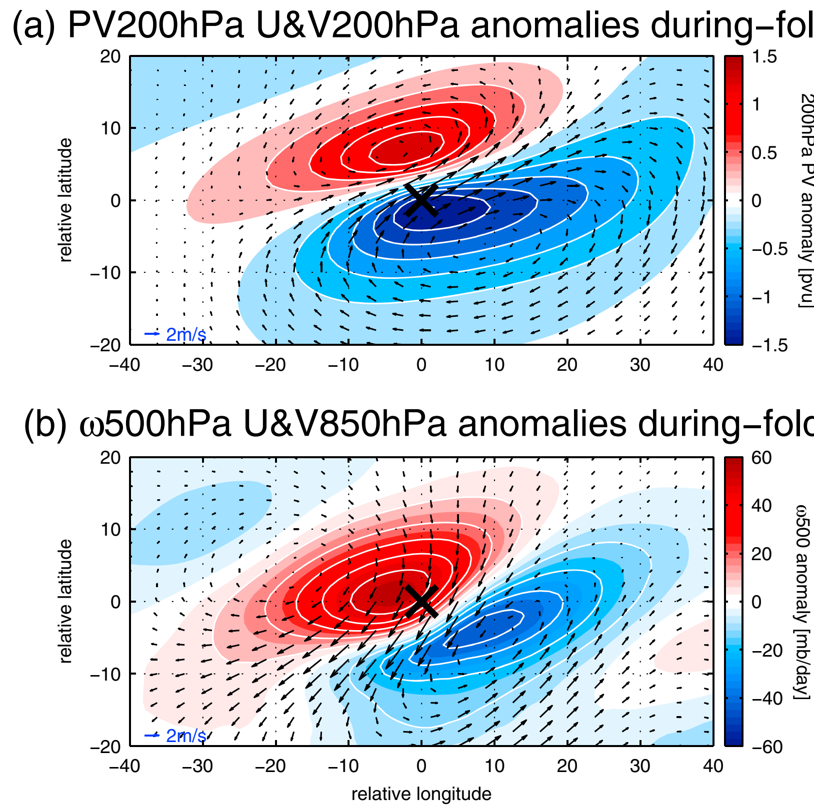

Figure 4. Composites of (a) 200 hPa potential vorticity (PV) anomaly (in unit of potential vorticity unit (PVU), plotted in color shadings and contours with CI = 0.25 PVU) and 200 hPa horizontal velocity anomaly (vectors) and (b) 500 hPa vertical velocity anomaly (in unit of mb/d, plotted in color shadings and contours with CI = 10 mb/d) and 850 hPa horizontal velocity anomaly (vectors) in idealized 7.5 K run. Black cross at the center highlights the tropopause fold location and both (a) and (b) are shown as a function of relative longitude and relative latitude. The results are all statistically significant at the 95% confidence level.

in closer proximity to the upper-level anticyclone. Although the investigation of RWB dynamics is beyond the scope of this study, the regression results suggest that the monsoon circulation plays an important role in controlling the occurrence of both the tropopause folds and RWB.

Therefore, both tropopause folds and RWB likely occur as a result of monsoon dynamics and this is summarized by a schematic in Figure 5c. While tropopause folds occur in conjunction with strong descent and strong upper-level northeastward flow, AWB takes place both downstream and upstream of the upper-level anticyclone associated with southwestward flow.

3.3. Impact on Extreme Rainfall Events

As discussed in section 1, previous studies have suggested the possible contribution of tropopause folds to rapid cyclogenesis and thus severe weather events. On the other hand, the subsidence associated with folds, as discussed in previous section, and also resulting dry air intrusion from the stratosphere seem to imply that it is unlikely that folds can instigate severe weather events (e.g., Fadnavis & Chattopadhyay, 2017; Mapes & Zuidema, 1996). Therefore, here we examine the impact of tropopause folds on extreme rainfall events using idealized model experiments.

In particular, we define a ratio $FR = \frac{P(\mathrm{PRECT} \geq \mathrm{threshold} \mid \mathrm{folds})}{P(\mathrm{PRECT} \geq \mathrm{threshold})}$, which compares the likelihood of extreme rainfall events given the occurrence of tropopause folds to that under normal conditions. The existence of folds increases (or decreases) the likelihood of extreme rainfall as compared to normal conditions if FR is larger (or smaller) than 1. Here the threshold of extreme rainfall is set to be 95th percentile, as an example (similar results are found for other thresholds; not shown). Figure 6 shows the impact of tropopause folds on extreme rainfall before, during and after the occurrence of folds. During folds, the frequency of extreme rainfall is significantly reduced (about halving the likelihood) at and upstream of the folds, likely due to the descending

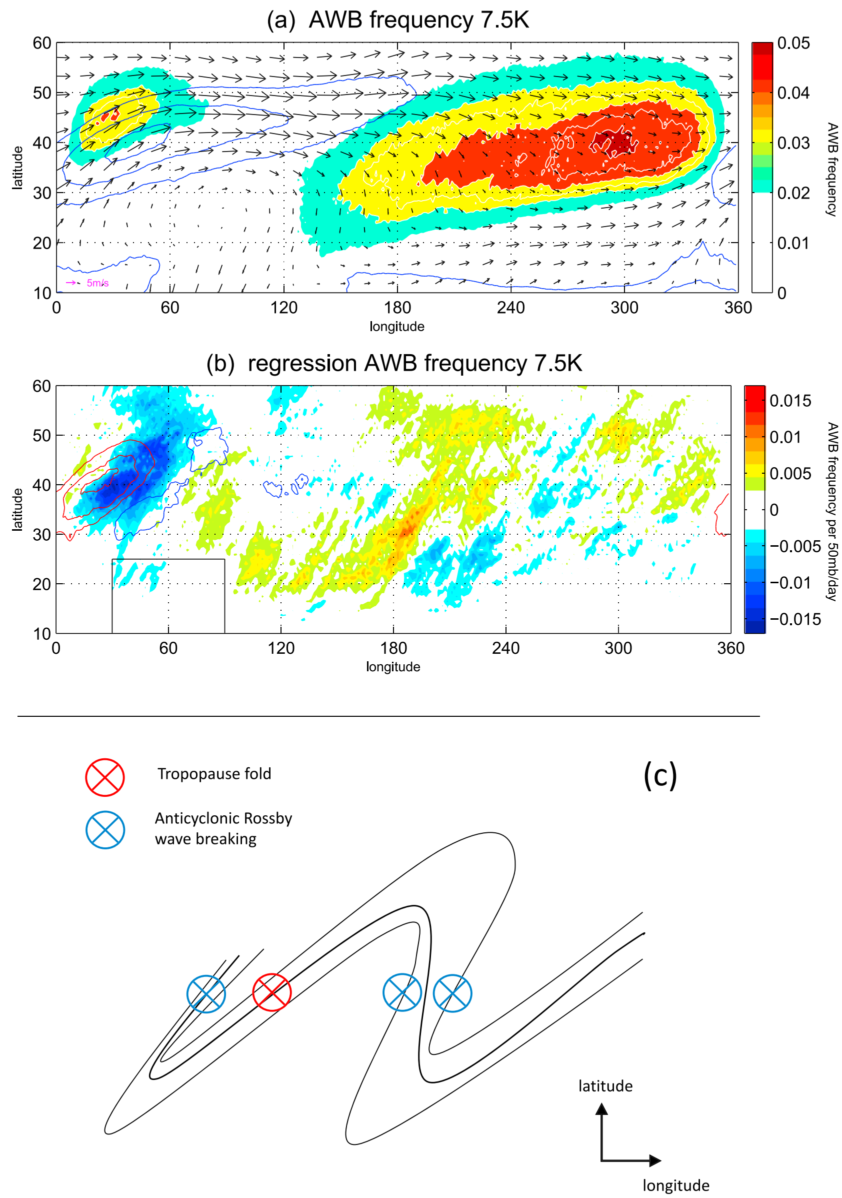

Figure 5. (a) Frequency of anticyclonic wave breaking (AWB) (color shadings and white contours with CI = 0.005) and tropopause folds (blue contours with CI = 0.05) in idealized 7.5 K aquaplanet experiment. Also plotted are climatological 200 hPa horizontal velocity fields (vectors). (b) Regression of AWB and tropopause folds on 500 hPa vertical velocity averaged over the black box (30–90°E and 10–25°N). The regression results for AWB are shown in color shadings, and the unit is per 50 mb/d. The regression results for tropopause folds are shown in contours with CI = 0.025 per 50 mb/d and red for positive values and blue for negative values. The regression results are all statistically significant at the 95% confidence level. Figures 5a and 5b are similar to Figure 3b and are shifted by 120° longitude to the west as compared to Figure 1. (c) Schematic showing the potential vorticity contours and occurrence of tropopause folds and AWB. Tropopause folds occur due to strong descent and strong northeastward flow, while AWB takes place downstream and, to a lesser extent, upstream with southwestward flow.

motion associated with the folds. However, the likelihood of extreme rainfall is largely increased (almost doubling the likelihood) downstream of the folds likely associated with the ascent downstream. Previous studies also found similar responses in convection, and, for example, Allen et al. (2009) found convection inhibition in the dry pool itself associated with tropopause folds but convection promotion at the leading edge of the dry slot in case studies from observations. And in our idealized model experiment, this suppression upstream and promotion downstream is seen to persist for at least 1–2 days after the occurrence of folds.

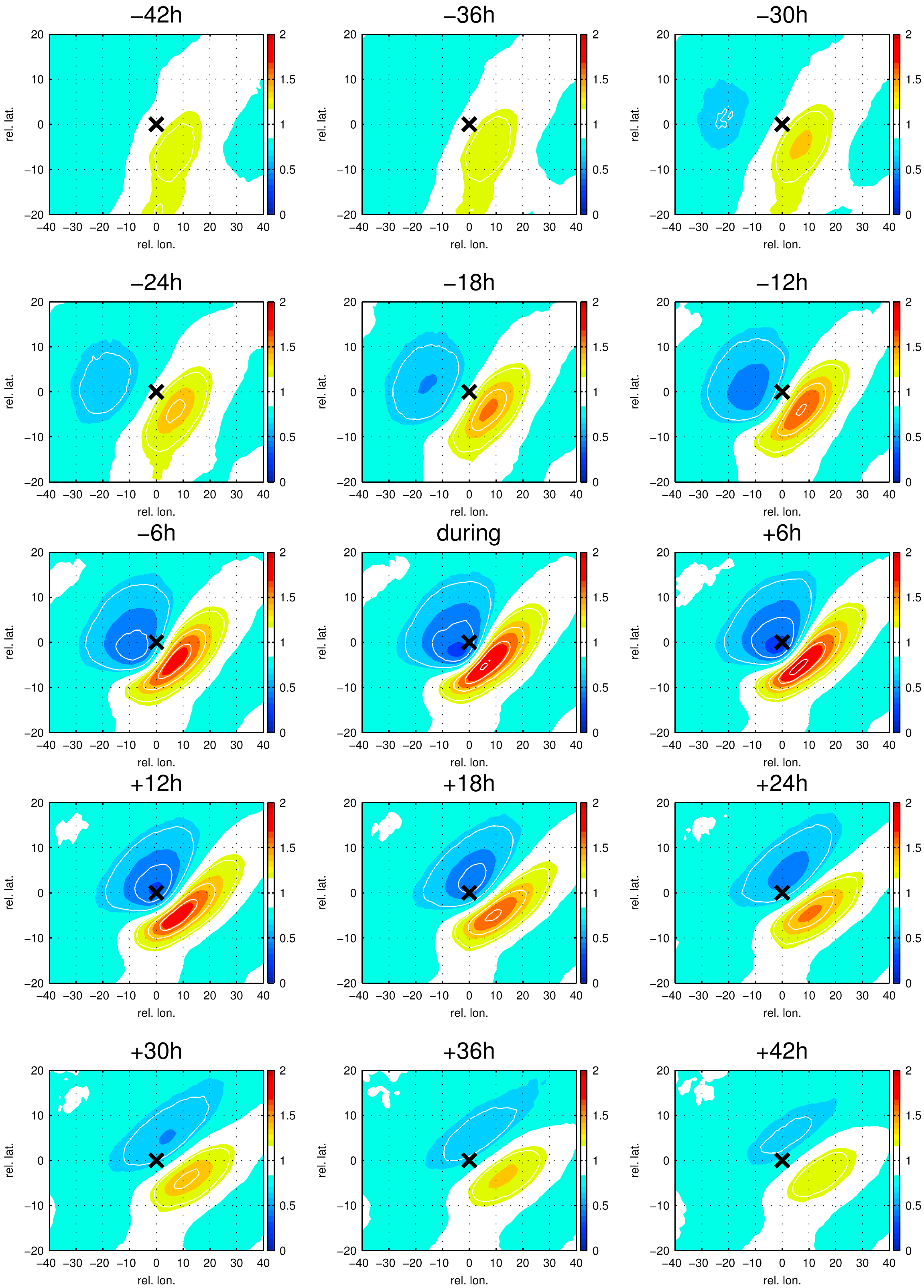

Figure 6. The impact of folds on extreme precipitation measured by $FR = \frac{P(\mathrm{PRECT} \geq \mathrm{threshold} \mid \mathrm{folds})}{P(\mathrm{PRECT} \geq \mathrm{threshold})}$ where threshold is set to be 95th percentile here shown in color shadings and white contours with CI = 0.25 in 7.5 K run. The results are shown every 6-hourly before, during, and after the occurrence of tropopause folds. The results are all statistically significant at the 95% confidence level. Black cross at the center highlights the tropopause fold location, and the plots are shown as a function of relative longitude and relative latitude.

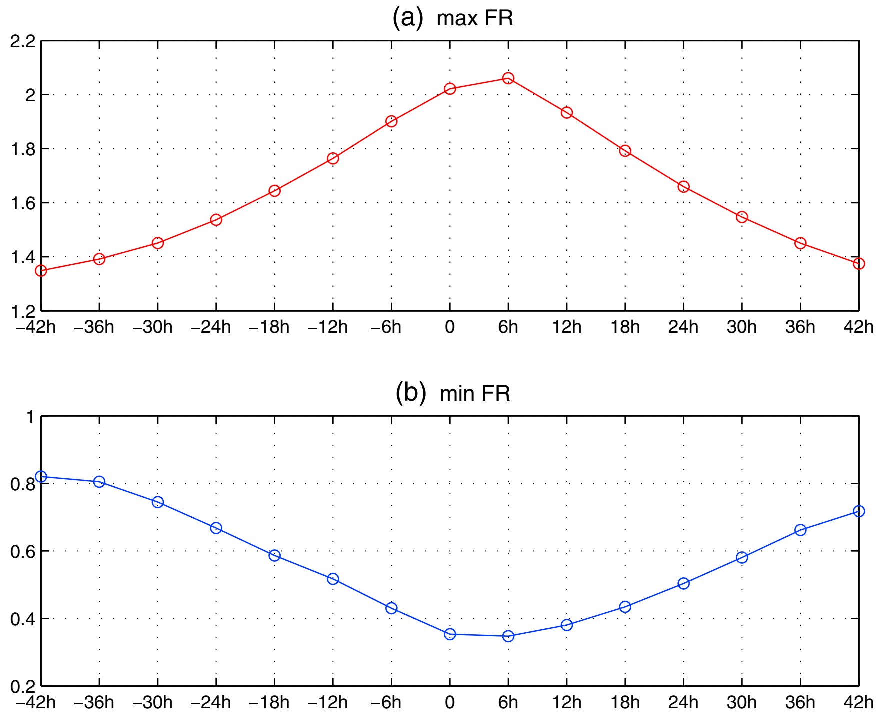

Figure 7. Six-hourly evolution of (a) maximum and (b) minimum of *FR* in 7.5 K run. The results are all statistically significant at the 95% confidence level.

Figure 7 further shows the 6-hourly evolution of the maximum and minimum of *FR*. It is interesting to note that both the maximum and minimum of the likelihood are reached 6 h after the occurrence of folds. This result is statistically significant at the 95% confidence level (not shown) and suggests a positive feedback between extreme ascent and rainfall downstream and tropopause folds. It is well known that an upper-level positive PV anomaly and a lower-level positive PV anomaly tend to phase lock, mutually intensify, and promote cyclogenesis, which is likely what happens here between tropopause folds and extreme rainfall events (e.g., Bluestein, 1993; Bretherton, 1966; Hoskins et al., 1985; Hoskins & Berrisford, 1988; a schematic of cyclogenesis associated with an upper-level PV anomaly can be seen in Figure 21 of Hoskins et al., 1985). An intensified low-level cyclonic circulation associated with the monsoon circulation can generate a strong descent on the northwestern side, which results in tropopause folds. Positive PV anomaly is then advected from the stratosphere during folds and causes the isentropic surfaces to bow toward it, leading to increased static stability toward positive PV anomaly while decreased static stability both above and below and thus further intensifies the ascending motion and rainfall. Figure 8 shows the evolution of potential temperature surfaces at about 5°S relative latitude where maximum extreme rainfall takes place. As can be seen, the isentropic surfaces in the lower troposphere are tilted downstream of the folds, which suggests decreased static stability and is consistent with increased frequency of extreme rainfall in the region. It is noted that the lower tropospheric isentropic surfaces are the most tilted during, 6 h, and 12 h after the occurrence of folds. Similar results are found at around 0°N relative latitude (see Figure S3 in the supporting information).

Although the occurrence of tropopause folds likely increases the probability of extreme rainfall downstream, the circulation system is strongly coupled between the lower and upper troposphere and the explicit role of folds alone on lower tropospheric circulation would need additional analysis such as PV inversion (e.g., Coronel et al., 2015; Griffiths et al., 2000). Such PV inversion analysis was done, for instance, by Coronel et al. (2015) where they examined the role of upper-level PV and moist processes in idealized surface cyclones and found a stronger surface cyclone with upper-level PV included than without.

Therefore, in summary, the idealized model experiments reveal that the occurrence of tropopause folds significantly decreases the likelihood of extreme rainfall events both at and upstream of the folds while it significantly increases the likelihood downstream. The results also suggest a positive feedback between extreme

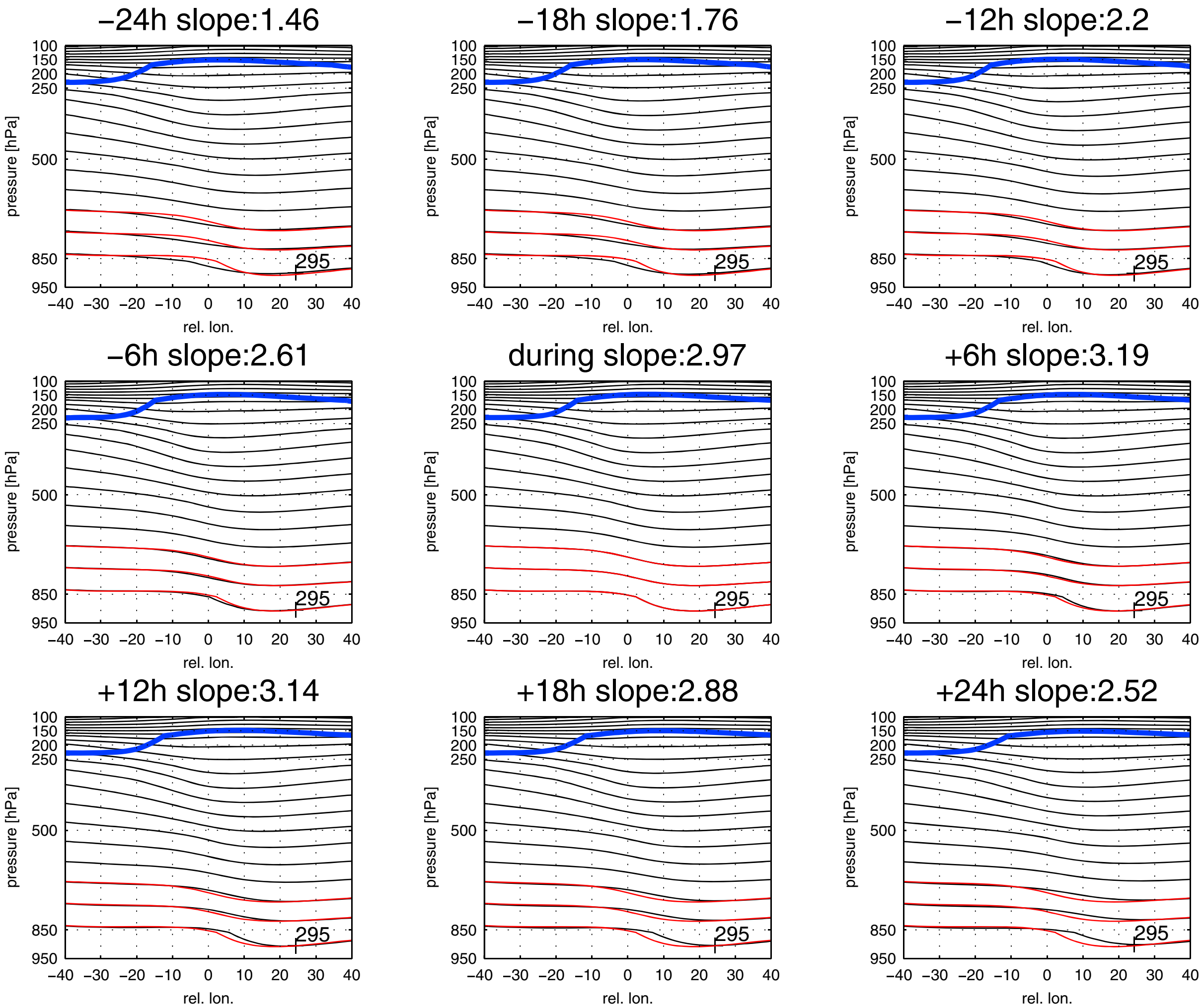

Figure 8. Cross section of potential temperature surfaces at relative latitude 5°S where maximum extreme rainfall occurs as a function of relative longitude and pressure level (black contours with CI = 5 K) every 6-hourly before, during, and after the occurrence of tropopause folds in 7.5 K run. The results focus on 1 day before and 1 day after the occurrence of folds. The numbers in the title indicate the isentropic slopes (in unit of hPa per degree longitude) at 295 K surface and averaged downstream 0–20° relative longitude. Red contours are identical in all subplots and show the lower tropospheric isentropic surfaces during the occurrence of folds as a reference. Blue contours plot the 2 PVU surfaces.

rainfall and tropopause folds, that is, while tropopause folds occur as a result of intensified monsoon circulation, the resulting upper tropospheric positive PV anomaly can modify the isentropic surfaces, decrease the static stability in the lower troposphere, and further promote the ascending motion and rainfall.

3.4. Response to Monsoon Intensity

Finally, we use idealized aquaplanet model experiments to show the sensitivity of the tropopause folds to monsoon intensity. Figure 9 shows the simulated fold frequency in 5 K, 7.5 K, and 10 K experiments. As can be seen, fold frequency increases significantly from 5 K to 7.5 K run, accompanied by significant intensified subsidence. From 7.5 K to 10 K run, folds have about the same magnitude of frequency but shift westward, which follows the westward shift of the subsidence. The change in tropopause fold frequency in response to anthropogenic forcing and changing monsoon intensity has a lot of implications for the stratosphere-troposphere transport of ozone and other chemical constituents and will be further studied in future work.

4. Conclusions and Discussion

Using a set of idealized aquaplanet model experiments forced with localized surface heating, we have demonstrated that tropopause folds occur because of monsoon dynamics during northern summer. More specifically, tropopause folds tend to occur on the northwestern side of the upper-level anticyclone associated

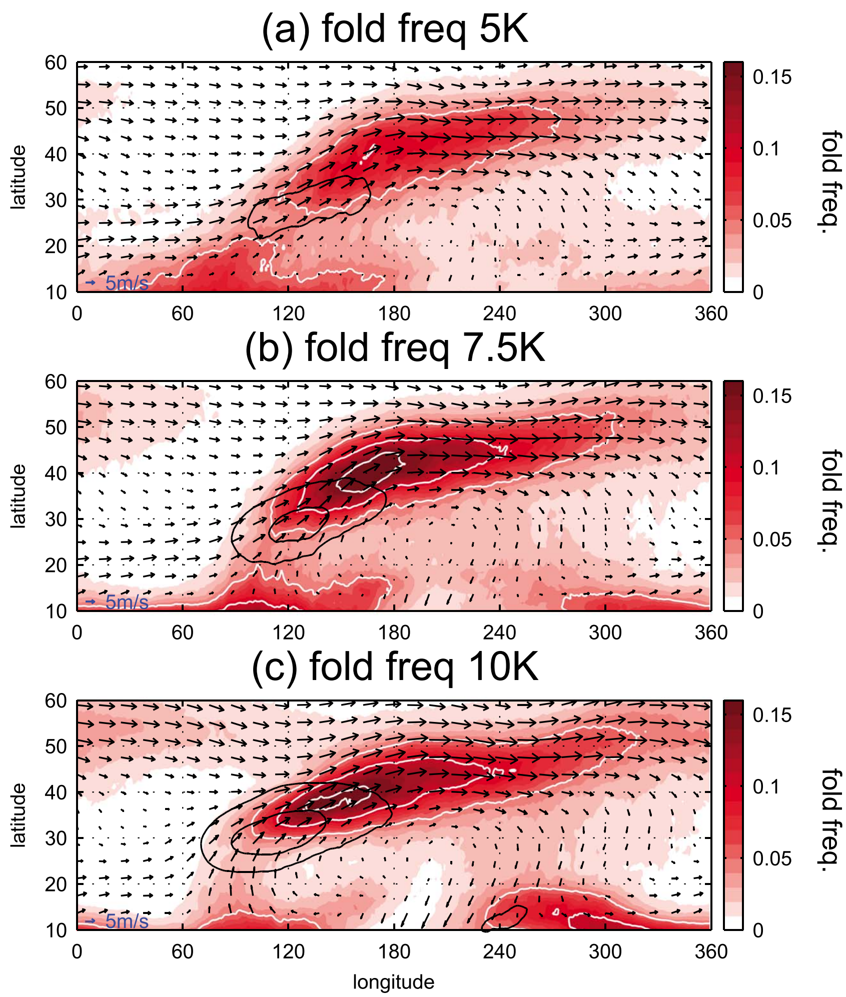

Figure 9. Tropopause fold frequency in (a) 5 K, (b) 7.5 K, and (c) 10 K experiments shown in color shadings and white contours with CI = 0.05. Also plotted are 200 hPa horizontal velocity fields (vectors) and 500 hPa vertical velocity (in unit of mb/d, plotted in black contours with CI = 25 mb/d).

with large-scale subsidence. Folds are typically seen to take place when there is an intensified subsidence associated with an intensified monsoon circulation. We also note that tropopause folds and AWB do not happen in the same geographical location, and while tropopause folds occur on the northwestern side of the upper-level anticyclone, AWB takes place downstream and to a lesser extent upstream. In addition, we have also quantified the impact of tropopause folds on extreme precipitation and we summarize the key conclusions in a schematic in Figure 10. As shown in Figure 10, we have found that while the likelihood of extreme rainfall is largely decreased at and upstream of the folds, the likelihood is significantly increased downstream. This pattern of suppression of extreme rainfall upstream while promotion downstream is seen to persist for 1–2 days, suggesting that a positive feedback between ascent downstream and tropopause folds is likely to play a role. As intensified monsoon circulation causes tropopause folds, the resulting positive PV anomaly associated with folds can lead to a decrease of static stability in the lower troposphere and further promote ascent and rainfall. Finally, tropopause folds also vary with monsoon intensity, that is, the frequency of folds significantly increases from weak to medium monsoon intensity and then saturates from medium to strong monsoon intensity with a shift in location toward the west.

While the aquaplanet model experiments provide significant insights into the mechanisms responsible for the occurrence of tropopause folds and its impact on extreme weather events, there are a couple of caveats worth mentioning. First, convection in Community Atmosphere Model version 5, or state-of-the-art atmospheric general circulation models in general, is highly parameterized, and frontal systems that are potentially important for folds (e.g., Keyser & Shapiro, 1986; Rao & Kirkwood, 2005) are not explicitly resolved. This study

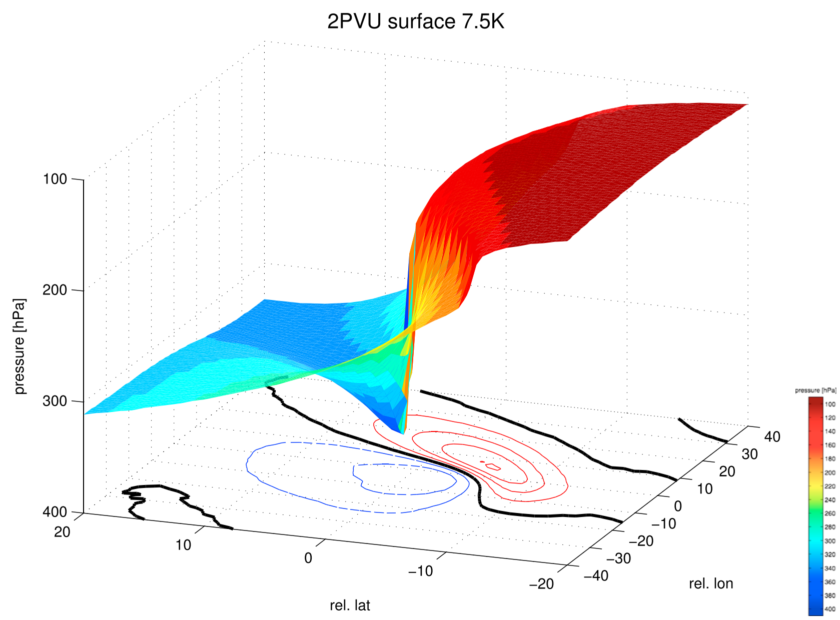

Figure 10. Similar to Figure 6 but a three-dimensional view of 2 PVU surface (color shadings) during the occurrence of tropopause folds. The contours plot the impact of folds on extreme precipitation measured by *FR* with blue contours for $FR < 1$, red for $FR > 1$, and black thick line for $FR = 1$ with CI = 0.25.

instead presents a picture of the interactions between large-scale circulation patterns and tropopause folds. Second, although the occurrence of tropopause folds likely increases the probability of extreme rainfall downstream, it is important to keep in mind that the lower and upper tropospheric circulation are strongly coupled together and it is not easy to untangle the two. However, previous studies have used PV inversion to examine the role of upper-level PV on surface cyclogenesis and found significant intensification of surface cyclones due to upper-level positive PV (e.g., Coronel et al., 2015; Griffiths et al., 2000).

The results highlight a strong linkage between the Asian summer monsoon circulation and tropopause fold activity over the eastern Mediterranean and the Middle East and suggest changes in fold frequency with changing monsoon intensity. Therefore, future work will be devoted to investigating the future changes in tropopause folds and resulting changes in stratosphere-to-troposphere transport of ozone and other chemical constituents as a consequence of anthropogenic forcing and changing monsoon intensity. Furthermore, the idealized simulations also demonstrate a potentially significant impact of tropopause folds on extreme rainfall events. The results highlight the need to consider upper troposphere and lower stratosphere processes in studies of convection over the summer monsoon regions.

Acknowledgments
The authors thank helpful discussions with Bill Randel, Joowan Kim, and Steven Feldstein during the AMS AOFD meeting. We thank the ECMWF for providing the ERA-Interim reanalysis data set. The ERA-Interim data used in this paper are available at http://apps.ecmwf.int/datasets/data/interim-full-daily/levtype=ml/.om The computations were carried out with high-performance computing support provided by NCAR's Computational and Information Systems Laboratory, which is sponsored by the National Science Foundation (NSF). The data produced for and analyzed in this paper are archived on the High Performance Storage System (HPSS) at NCAR and are freely available via contacting Y. W. (yutianwu@ldeo.columbia.edu). Y. W. is supported, in part, by the NSF award AGS-1653878. G. C. is supported by the NSF awards AGS-1742178 and AGS-1608775. P. Z. is supported by the NSFAGS-1406962.

References

Allen, G., Vaughan, G., Brunner, D., May, P. T., Heyes, W., Minnis, P., & Ayers, J. K. (2009). Modulation of tropical convection by breaking Rossby waves. *Quarterly Journal of the Royal Meteorological Society*, *135*, 125–137. https://doi.org/10.1002/qj.349

Bluestein, H. B. (1993). *Synoptic-dynamic meteorology in midlatitudes: Volume II: Observations and theory of weather systems* (1st ed.). New York: Oxford University Press.

Bourqui, M. S., & Trepanier, P.-Y. (2010). Descent of deep stratospheric intrusions during the IONS August 2006 campaign. *Journal of Geophysical Research*, *115*, D18301. https://doi.org/10.1029/2009JD013183

Bretherton, F. P. (1966). Baroclinic instability and the short wavelength cut-off in terms of potential vorticity. *Quarterly Journal of the Royal Meteorological Society*, *92*, 335–345. https://doi.org/10.1002/qj.49709239303

Browning, K. A., & Golding, B. W. (1995). Mesoscale aspects of a dry intrusion within a vigorous cyclone. *Quarterly Journal of the Royal Meteorological Society*, *121*, 463–493. https://doi.org/10.1002/qj.49712152302

Browning, K. A., & Reynolds, R. (1994). Diagnostic study of a narrow cold-frontal rainband and severe winds associated with a stratospheric intrusion. *Quarterly Journal of the Royal Meteorological Society*, *120*, 235–257. https://doi.org/10.1002/qj.49712051602

Coronel, B., Ricard, D., Riviere, G., & Arbogast, P. (2015). Role of moist processes in the tracks of idealized midlatitude surface cyclones. *Journal of the Atmospheric Sciences*, *72*, 2979–2996. https://doi.org/10.1175/JAS–D–14–0337.1

Danielsen, E. F. (1968). Stratospheric-tropospheric exchange based on radioactivity, ozone and potential vorticity. *Journal of the Atmospheric Sciences*, *25*, 502–518.

Dee, D. P., Uppala, S. M., Simmons, A. J., Berrisford, P., Poli, P., Kobayashi, S., … Vitart, F. (2011). The ERA-Interim reanalysis: Configuration and performance of the data assimilation system. *Quarterly Journal of the Royal Meteorological Society*, *137*, 553–597. https://doi.org/10.1002/qj.828

Fadnavis, S., & Chattopadhyay, R. (2017). Linkages of subtropical stratospheric intraseasonal intrusions with Indian summer monsoon deficit rainfall. *Journal of Climate*, *30*, 5083–5095. https://doi.org/10.1175/JCLI–D–16–0463.1

Gill, A. E. (1980). Some simple solutions for heat-induced tropical circulation. *Quarterly Journal of the Royal Meteorological Society*, *106*, 447–462. https://doi.org/10.1002/qj.49710644905

Goering, M. A., Gallus, W. A. Jr., Olsen, M. A., & Stanford, J. L. (2001). Role of stratospheric air in a severe weather event: Analysis of potential vorticity and total ozone. *Journal of Geophysical Research*, *106*(D11), 11813–11823. https://doi.org/10.1029/2000JD900651

Griffiths, M., Thorpe, A. J., & Browning, K. A. (2000). Convective destabilization by a tropopause fold diagnosed using potential-vorticity inversion. *Quarterly Journal of the Royal Meteorological Society*, *126*, 125–144. https://doi.org/10.1002/qj.49712656207

Holton, J. R., Haynes, P. H., McIntyre, M. E., Douglass, A. R., Rood, R. B., & Pfister, L. (1995). Stratosphere-troposphere exchange. *Reviews of Geophysics*, *33*(4), 403–440. https://doi.org/10.1029/95RG02097

Homeyer, C. R., & Bowman, K. P. (2013). Rossby wave breaking and transport between the tropics and extratropics above the subtropical jet. *Journal of the Atmospheric Sciences*, *70*, 607–626. https://doi.org/10.1175/JAS–D–12–0198.1

Hoskins, B., & Berrisford, P. (1988). A potential vorticity perspective of the storm of 15–16 October 1987. *Weather*, *43*, 122–129. https://doi.org/10.1002/j.1477–8696.1988.tb03890.x

Hoskins, B. J., McIntyre, M. E., & Robertson, A. W. (1985). On the use and significance of isentropic potential vorticity maps. *Quarterly Journal of the Royal Meteorological Society*, *111*, 877–946. https://doi.org/10.1002/qj.49711147002

Keyser, D., & Shapiro, M. A. (1986). A review of the structure and dynamics of upper-level frontal zones. *Monthly Weather Review*, *114*, 452–499.

Kourtidis, K., Zerefos, C., Rapsomanikis, S., Simeonov, V., Balis, D., Perros, P. E., … Drakou, R. (2002). Regional levels of ozone in the troposphere over eastern Mediterranean. *Journal of Geophysical Research*, *107*(D18), 8140. https://doi.org/10.1029/2000JD000140

Kunz, A., Sprenger, M., & Wernli, H. (2015). Climatology of potential vorticity streamers and associated isentropic transport pathways across PV gradient barriers. *Journal of Geophysical Research: Atmospheres*, *120*, 3802–3821. https://doi.org/10.1002/2014JD022615

Lamarque, J.-F., & Hess, P. G. (1994). Cross-tropopause mass exchange and potential vorticity budget in a simulated tropopause folding. *Journal of the Atmospheric Sciences*, *51*(15), 2246–2269.

Lelieveld, J., Berresheim, H., Borrmann, S., Crutzen, P. J., Dentener, F. J., Fischer, H., … Ziereis, H. (2002). Global air pollution crossroads over the Mediterranean. *Science*, *298*, 794–799. https://doi.org/10.1126/science.1075457

Lu, J., Sun, L., Wu, Y., & Chen, G. (2014). The role of subtropical irreversible PV mixing in the zonal mean circulation response to global warming-like thermal forcing. *Journal of Climate*, *27*, 2297–2316. https://doi.org/10.1175/JCLI–D–13–00372.1

Mapes, B. E., & Zuidema, P. (1996). Radiative-dynamical consequences of dry tongues in the tropical troposphere. *Journal of the Atmospheric Sciences*, *53*, 620–638. https://doi.org/10.1175/1520–0469(1996)053<0620:RDCODT>2.0.CO;2

Neale, R. B., Richter, J. H., Conley, A. J., Park, S., Lauritzen, P. H., Gettelman, A., & Williamso, D. L. (2012). Description of the NCAR Community Atmosphere Model (CAM 5.0) (*NCAR Tech*). Boulder, Colorado, USA: NCAR/TN–4861STR.

Postel, G. A., & Hitchman, M. H. (1999). A climatology of Rossby wave breaking along the subtropical tropopause. *Journal of the Atmospheric Sciences*, *56*, 359–373. https://doi.org/10.1175/1520–0469(1999)056<0359:ACORWB>2.0.CO;2

Rao, T. N., & Kirkwood, S. (2005). Characteristics of tropopause folds over Arctic latitudes. *Journal of Geophysical Research*, *110*, D18102. https://doi.org/10.1029/2004JD005374

Reed, R. J. (1955). A study of a characteristic type of upper-level frontogenesis. *Journal of the Atmospheric Sciences*, *12*, 226–237.

Reed, R. J., & Danielsen, E. F. (1959). Fronts in the vicinity of the tropopause. *Archiv für Meteorologie, Geophysik und Bioklimatologie, Serie A*, *11*(1), 1–17. https://doi.org/10.1007/BF02247637

Rivière, G. (2009). Effect of latitudinal variations in low-level baroclinicity on eddy life cycles and upper-tropospheric wave-breaking processes. *Journal of the Atmospheric Sciences*, *66*, 1569–1592. https://doi.org/10.1175/2008JAS2919.1

Rodwell, M. J., & Hoskins, B. J. (1996). Monsoons and the dynamics of deserts. *Quarterly Journal of the Royal Meteorological Society*, *122*, 1385–1404. https://doi.org/10.1002/qj.49712253408

Rodwell, M. J., & Hoskins, B. J. (2001). Subtropical anticyclones and summer monsoons. *Journal of Climate*, *14*, 3192–3211. https://doi.org/10.1175/1520-0442(2001)014<3192:SAASM>2.0.CO;2

Roelofs, G. J., & Lelieveld, J. (1997). Model study of the influence of cross-tropopause O3 transports on tropospheric O3 levels. *Tellus B*, *49*, 38–55. https://doi.org/10.1034/j.1600–0889.49.issue1.3.x

Roelofs, G. J., Scheeren, H. A., Heland, J., Ziereis, H., & Lelieveld, J. (2003). A model study of ozone in the eastern Mediterranean free troposphere during MINOS (August 2001). *Atmospheric Chemistry and Physics*, *3*, 1199–1210.

Shapiro, M. A. (1980). Turbulent mixing within tropopause folds as a mechanism for the exchange of chemical constituents between the stratosphere and troposphere. *Journal of the Atmospheric Sciences*, *37*, 994–1004.

Shapiro, M. A. (1981). Frontogenesis and geostrophically forced secondary circulations in the vicinity of jet stream-frontal zone systems. *Journal of the Atmospheric Sciences*, *38*, 954–973.

Shaw, T. A. (2014). On the role of planetary-scale waves in the abrupt seasonal transition of the Northern Hemisphere general circulation. *Journal of the Atmospheric Sciences*, *71*, 1724–1746.

Skerlak, B., Sprenger, M., Pfahl, S., Tyrlis, E., & Wernli, H. (2015). Tropopause folds in ERA-Interim: Global climatology and relation to extreme weather events. *Journal of Geophysical Research: Atmospheres*, *120*, 4860–4877. https://doi.org/10.1002/2014JD022787

Sprenger, M., Maspoli, M. Croci, & Wernli, H. (2003). Tropopause folds and cross-tropopause exchange: A global investigation based upon ECMWF analyses for the time period March 2000 to February 2001. *Journal of Geophysical Research*, *108*(D12), 8518. https://doi.org/10.1029/2002JD002587

Stohl, A., Bonasoni, P., Cristofanelli, P., Collins, W., Feichter, J., Frank, A., … Zerefos, C. (2003). Stratosphere-troposphere exchange: A review, and what we have learned from STACCATO. *Journal of Geophysical Research*, *108*(D12), 8516. https://doi.org/10.1029/2002JD002490

Strong, C., & Magnusdottir, G. (2008). Tropospheric Rossby wave breaking and the NAO/NAM. *Journal of the Atmospheric Sciences*, *65*, 2861–2876. https://doi.org/10.1175/2008JAS2632.1

Thorpe, A. J. (1997). Attribution and its application to mesoscale structure associated with tropopause folds. *Quarterly Journal of the Royal Meteorological Society*, *123*, 2377–2399. https://doi.org/10.1002/qj.49712354411

Tyrlis, E., Skerlak, B., Sprenger, M., Wernli, H., Zittis, G., & Lelieveld, J. (2014). On the linkage between the Asian summer monsoon and tropopause fold activity over the eastern Mediterranean and the Middle East. *Journal of Geophysical Research: Atmospheres*, *119*, 3202–3221. https://doi.org/10.1002/2013JD021113

Uccellini, L. W. (1990). Processes contributing to the rapid development of extratropical cyclones. In C. W. Newton & E. O. Holopainen (Eds.), *Extratropical cyclones. The Erik Palmén memorial volume* (pp. 81–105). Massachusetts: American Meteorological Society.

Wernli, H., Dirren, S., Liniger, M. A., & Zillig, M. (2002). Dynamical aspects of the life cycle of the winter storm 'Lothar' (24-26 December 1999). *Quarterly Journal of the Royal Meteorological Society*, *128*, 405–429. https://doi.org/10.1256/003590002321042036

Wu, Y., & Shaw, T. A. (2016). The impact of the Asian summer monsoon circulation on the tropopause. *Journal of Climate*, *29*, 8689–8701.

Yang, H., Chen, G., Tang, Q., & Hess, P. (2016). Quantifying isentropic stratosphere-troposphere exchange of ozone. *Journal of Geophysical Research: Atmospheres*, *121*, 3372–3387. https://doi.org/10.1002/2015JD024180

Zhang, Q., Wu, G., & Qian, Y. (2002). The bimodality of the 100 hPa South Asia High and its relationship to the climate anomaly over East Asia in summer. *Journal of the Meteorological Society of Japan. Ser. II*, *80*, 733–744. https://doi.org/10.2151/jmsj.80.733